JOURNAL OF MATERIALS SCIENCE 22 (1987) 4388–4394

Surface crystallization of melt-spun $Pd_{40}Ni_{40}P_{20}$ glass

A. GARCIA ESCORIAL
Centro Nacional de Investigaciones Metalurgicas, Avenida de Gregorio del Amo 8, 28040 Madrid, Spain

A. L. GREER
Department of Materials Science and Metallurgy, University of Cambridge, Pembroke Street, Cambridge, CB2 3QZ, UK

The crystallization of $Pd_{40}Ni_{40}P_{20}$ glass, produced by melt-spinning in air, has been studied by optical metallography. Crystallization is predominantly from the surface and is more prevalent on the wheel-side. The non-uniformity is attributed to variation in quench rate during production. A three-stage anneal permits crystals which have nucleated at the surface to be identified and their size distribution to be analysed. The surface nucleation is heterogeneous and appears to be hindered by mild oxidation. The annealing atmosphere markedly affects the surface crystallization behaviour, as does removal of the original ribbon surface. When nucleation is sparse, partial crystallization causes the development of noticeable relief on the sample surfaces.

1. Introduction

Surface crystallization of metallic glasses has not been studied as much as its importance would merit. The phenomenon is significant in considering the stability of metallic glasses in potential applications, because the glasses may have less resistance to surface crystallization than to internal crystallization. Furthermore, the surface crystallization may affect not only surface-specific properties such as corrosion and catalytic behaviour. For example, the stresses generated by surface crystalline layers may affect magnetic properties [1]. On the other hand, surface crystallization may be put to use because it offers special opportunities for microstructural control.

There are several reasons to expect preferred crystallization at the surface of a glassy sample. Crystal nucleation and growth may be favoured by surface energies; such effects are important, for example, in the secondary recrystallization of grain-oriented silicon steel [2]. The stresses caused by the change of volume on crystallization can be more easily relieved at a surface, and this is clearly illustrated by the enhanced crystallization at the surfaces of amorphous selenium [3]. Surface crystallization may also be accelerated by faster atomic transport on a free surface, but this effect will be ruled out in most cases by oxidation. Indeed, preferential oxidation, causing a change in surface composition, is probably the major reason for surface crystallization in metallic glasses.

Köster [4] has shown that preferential oxidation of boron leads to the formation of α-Fe crystals on the surfaces of $Fe_{80}B_{20}$ glass. In the case of $Fe_{60}Ni_{20}B_{20}$ glass, preferential oxidation of iron leads not only to surface crystallization, but also to the formation of an orthorhombic phase, different from the tetragonal phase formed on internal crystallization [4]. The importance of preferential oxidation of iron was again demonstrated by a careful series of experiments on $Fe_{40}Ni_{40}B_{20}$ glass [4]. Electrochemical polishing removes iron and promotes uniform surface crystallization. This effect can be removed by ion-milling away the modified surface layer, or by diffusing iron into it. On the other hand, crystallization at a clean ion-milled surface can be promoted by diffusing nickel into it.

In the present work, the glass $Pd_{40}Ni_{40}P_{20}$ has been chosen for study because of its special characteristics, in particular its unusually high reduced glass transition temperature, $T_{rg} \approx 0.67$. The consequently low homogeneous crystal nucleation frequency permits glass formation at rates as low as $\sim 1\,K\,sec^{-1}$, if heterogeneous nucleation is avoided [5, 6], and minimum sample dimensions of ~ 1 cm can be achieved. The glass crystallizes to a eutectic mixture of three phases: a nickel-rich phosphide (orthorhombic, $a = 0.409$ nm, $b = 0.646$ nm, $c = 0.785$ nm, $Pd_{34}Ni_{45}P_{21}$); a metallic solid solution (fcc, $a = 0.372$ nm, $Pd_{40}Ni_{59}P_1$); and a palladium-rich phosphide (orthorhombic, $a = 0.515$ nm, $b = 0.584$ nm, $c = 0.750$ nm, $Pd_{68}Ni_{14}P_{18}$) [7]. Transmission electron microscopy [8] shows that the nickel- rich phosphide occurs as protruding needles oriented in the growth direction, with the other two phases in a fine "herringbone" lamellar pattern in between. It seems likely, therefore, that the nickel-rich phosphide is the first phase to nucleate. In any case, the growth rate of the ternary eutectic is exceedingly low [8], and this permits careful study of the crystallization kinetics. Of particular interest here is that the effective lack of homogeneous nucleation in this alloy allows heterogeneous nucleation to be examined in detail. This has been done for surface crystallization of ribbons melt-spun in air, and the results enable some conclusions

0022–2461/87 $03.00 + .12

to be drawn about the melt-spinning process. The standard annealing treatments were carried out on as-quenched ribbons under an argon atmosphere. However, extra insight was gained from the analysis of results on samples which had been pre-treated (chemically etched, ion-milled, or metal- coated), and which were annealed in other atmospheres (air, or vacuum).

2. Experimental methods

The $Pd_{40}Ni_{40}P_{20}$ (composition in atomic per cent) alloy was prepared from palladium powder (99.99%, from Aldrich Chemical Co. Ltd) and Ni_2P powder (99.9%, Ventron Alfa Products Ltd). The palladium powder was melted in an arc furnace under argon and formed into an ingot. The Ni_2P powder was similarly consolidated by melting in a fused silica capsule under vacuum (10^{-6} torr). The two ingots were alloyed by r.f. induction melting in a fused silica capsule under vacuum (10^{-6} torr). The resulting alloy was melt-spun in air to be a ribbon approximately 0.5 mm wide and 25 μm thick. The estimated cooling rate is $\sim 10^{-6}$ K sec^{-1}. The amorphicity of the ribbon was confirmed by X-ray diffraction (Cu$K\alpha$ radiation) and by differential scanning calorimetry (DSC) on a Dupont 990 instrument. The DSC results were in agreement with published data on this alloy [9].

Portions of the ribbon were sealed off under a controlled atmosphere in Pyrex capsules for annealing. The atmosphere was argon (99.999%, 240 torr), or vacuum (10^{-5} torr). The crystallization was followed by optical metallography after annealing. Where necessary, the samples were mounted in epoxy resin, mechanically polished to 0.05 μm, and then etched in dilute aqua regia (5 parts hydrochloric acid, 1 part nitric acid and 5 parts distilled water). It was found that the crystallization behaviour was different on the two sides of the ribbon. In this work these will be termed the air-side and the wheel-side (next to the wheel in melt-spinning). In the next section the initial results are reported separately for the two sides. X-ray diffraction was used to confirm that crystallization was occurring. The same phases were formed throughout, even when the behaviour on the two sides of the ribbon was quite different. The phases formed are those described in Section 1 [7].

3. Results and discussion

3.1. Air-side crystallization

The air-side of as-quenched ribbons is quite smooth, and this facilitates observation and analysis of surface crystallization. Fig. 1 is a series of optical micrographs showing increasing degrees of crystallization of the air-side. These samples were variously annealed under argon and then lightly etched. It is particularly evident in the early stages of the transformation (Figs 1a and b) that the distribution of crystals is not random; there is a tendency for the crystals to lie in lines approximately parallel to the length of the ribbon. Also, there is a greater concentration of crystals near the edge of the ribbon (Figs 1c and d).

In cross-section the crystalline regions are circular, suggesting spherical growth (with rate independent of direction) as seen by Drehman and Greer [9]. Careful examination (Fig. 1f) shows that the crystals appear to be of two kinds. In one kind, an internal structure of radial lines is visible; the others are darker with little internal contrast. As will be confirmed in Section 3.4, the former kind nucleated at the surface so that the centre of the growth pattern is visible, while the latter are the surface intersections of crystals which nucleated inside the ribbon. Such intersections on random sections can be and have been [8] used to derive the crystal size distribution in the bulk; the spherical growth arising from the eutectic decomposition of the amorphous phase makes the derivation comparatively straightforward. In this work, however, we are concerned only with crystals which nucleated at the free surface. Their size distribution after an anneal of 70 min at 623 K is shown in Fig. 2. Given eutectic decomposition, the isothermal growth rate is independent of time and the crystal radius is proportional to the time since nucleation. Fig. 2 indicates a decreasing nucleation rate. The decrease in the rate is much faster than would be caused by the decrease of the untransformed area fraction on the specimen surface, and is evidence for site saturation. This confirms that the surface nucleation is heterogeneous, as suggested by its non-random distribution. The crystal size distribution can be reasonably well fitted assuming a site population of $3.5 \times 10^8 m^{-2}$ and a constant heterogeneous nucleation frequency of $1.03 \times 10^{-3} sec^{-1}$ per site. Although detailed measurements at temperatures other than 623 K have not been attempted, the site population appears to be independent of temperature.

When the crystallized fraction becomes high, some surface relief develops on the samples, as seen in Fig. 1e. The remaining amorphous material (which must be essentially liquid) is drawn into the spaces between the growing crystals, indicating volume contraction on crystallization. Such an effect is visible only because of the remarkable resistance to crystallization of this alloy; even at elevated temperature, the density of crystal nuclei is very low. The surface relief is shown in more detail in Fig. 3. The raised lines in Fig. 3b may correspond to lines of nucleation events as seen in, for example, Fig. 1a. Liquid-like behaviour was also seen in DSC samples which flowed so that their base took up the ridged surface relief of the aluminium sample pan.

3.2. Wheel-side crystallization

Figs 4a and b show the wheel-side surface of ribbons which, as in the previous section, have been annealed in argon and then etched. The most obvious difference from the behaviour on the air-side of the ribbons is the high population of nuclei, leading to a high fraction crystallized. This is evident from a comparison of Figs 4a and b with Figs 1a and c, respectively, showing the two sides of similarly annealed ribbons. In some areas the nucleation is so copious that the surface is completely crystalline. It is still possible to see, however, that, as on the air-side, the nucleation is not random, but is concentrated in lines parallel to the ribbon length. A ridge pattern in this direction is visible

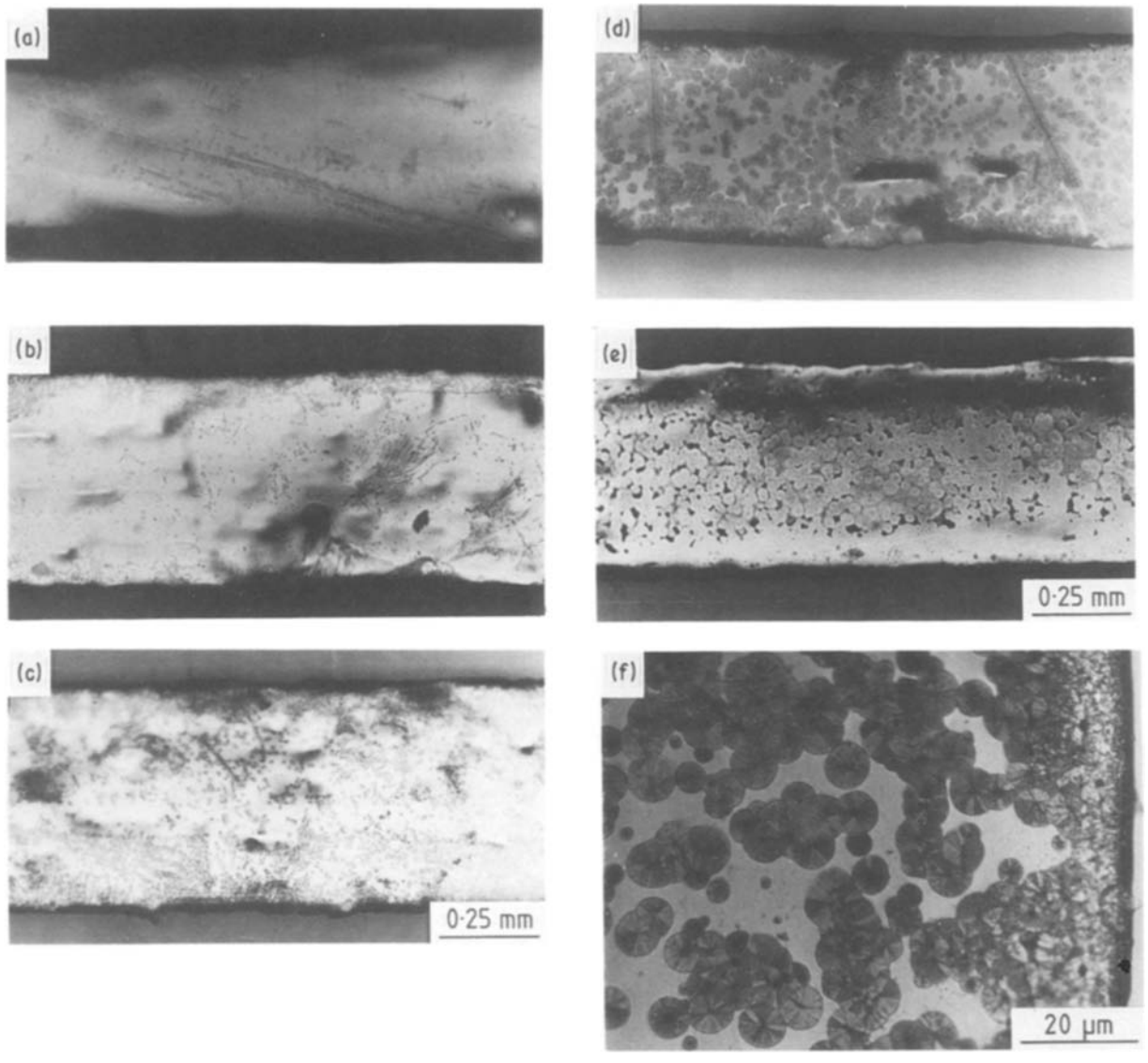

Figure 1 A series of optical micrographs of the etched air-side of melt-spun $Pd_{40}Ni_{40}P_{20}$ ribbon annealed in argon: (a) 23 min at 623 K; (b) 15 h at 583 K; (c) 2 h at 603 K; (d) 70 min at 623 K; (e) 75 h at 583 K; (f) close-up of c.

on the as-produced ribbon, and presumably results from polishing marks on the quenching wheel. It is difficult to tell from the line pattern whether the nucleation is preferred on areas of good or bad contact on the wheel. This is resolved by studying the depressions in the ribbon surface which are numerous on the wheel-side. They arise from gas entrapment between the ribbon and the wheel in melt-spinning. Fig. 4b shows that, apart from some sporadic events, nucleation does not occur on the surface of the depressions. Crystallization can be seen proceeding into the depressions from the surrounding transformed material. Thus nucleation occurs preferentially in areas where the surface of the ribbon was in contact with the wheel. This is opposite to the behaviour expected if the nucleation were influenced by quench rate, and it indicates the importance of heterogeneities at the surface. The nature of the surface modification will be considered in Section 3.7.

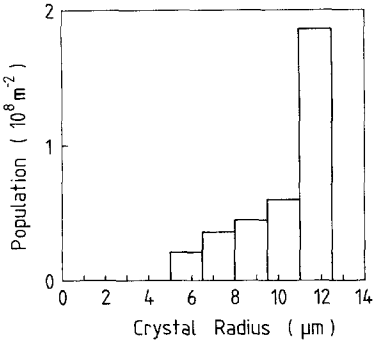

Figure 2 The size distribution of surface-nucleated crystals on the air-side of a ribbon annealed for 70 min at 623 K (cf. Fig. 1d).

3.3. Cross-sectional studies

Ribbons annealed in argon were sectioned in mounts, polished and etched in order to confirm and extend the surface studies. Figs 5a and b show, on the wheel-side, planar crystal growth from the copious nucleation, broken only at a few depressions. There is also growth from sporadic nucleation on the air-side, becoming more prevalent near the ribbon edges. Internal nucleation and growth can be seen, and some of the internally nucleated crystals do intersect the top surface as suggested in Section 3.1. Fig. 5c shows a very early stage of crystallization (corresponding to Fig. 4b); it is possible to resolve areas of transformation on the wheel-side, but it is confirmed that there are none on

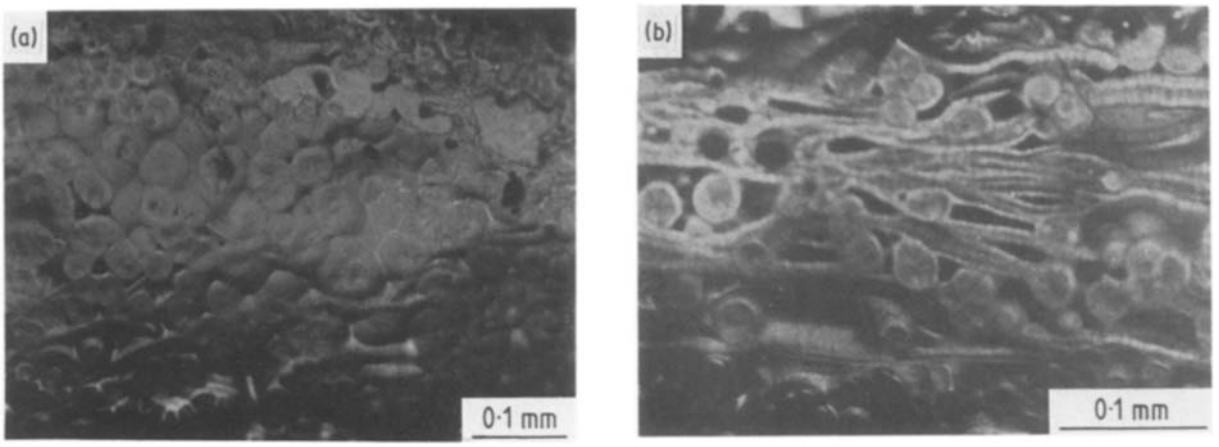

Figure 3 Optical micrographs of the surface relief which develops on the air-side of ribbons annealed in argon, in this case for 120 min at 653 K. The surfaces have not been etched.

the surface of the depression. (The depression in the air-side opposite is caused by the lower cooling rate in this region.)

The planar growth from the wheel side enables the crystal growth rate to be determined unambiguously as there are no problems with the interpretation of two-dimensional sections. The extent of growth as a function of time at, for example, 603 K is shown in Fig. 6. The isothermal growth is linear, as would be expected for a eutectic transformation in which the composition of the remaining amorphous phase is unaltered throughout. There appears to be no incubation period for the onset of growth. The growth rates, U, determined in this work (in the range 583 to 623 K) are in good agreement [8] with an Arrhenius extrapolation of the expression derived from differential scanning calorimetry measurements [9] at higher temperatures

$$U = (1.0 \times 10^{20}\,\mathrm{m\,sec^{-1}}) \exp(-3.49\,\mathrm{eV}/kT). \quad (1)$$

3.4. Three-stage annealing

It can be seen from earlier micrographs (e.g. Fig. 5a) that some internal structure in the crystalline areas can be resolved. Because the scale of a eutectic structure is expected to vary with the temperature at which it is grown, this suggests the possibility of distinguishing areas crystallized at different temperatures. A three-stage anneal was used to test this: 30 min at 623 K, 15 h at 583 K, and 30 min at 623 K, in argon. The first and third stages were chosen to be the same to enable a simple check that the extent of growth in each stage was the same.

Fig. 7a shows the air-side. In the large crystalline areas three growth rings can be distinguished. The extent of the first and third stages is the same. This confirms that the growth is linear and that it nucleated with little or no incubation period on the surface and not underneath. On the other hand, the smaller crystallized areas, which also appear darker, do not show the ring pattern, confirming that they are off-centre sections through larger spheres, i.e. that they were nucleated below the ribbon surface. Thus the selection of crystals for the size analysis in Section 3.1 is justified.

The cross-sections in Fig. 7b show some internal crystallites, but the ring pattern will not readily be visible unless they are sectioned close to their centre. On the other hand, the three growth stages can be seen in the planar crystallization from the wheel side. The first and third stages are again of equal extent, showing linear growth with negligible incubation period.

Figs 7a and b demonstrate the periodic changes in temperature during an anneal can be a useful way of marking stages in a crystal growth process. This can be especially important to interpreting two-dimensional sections.

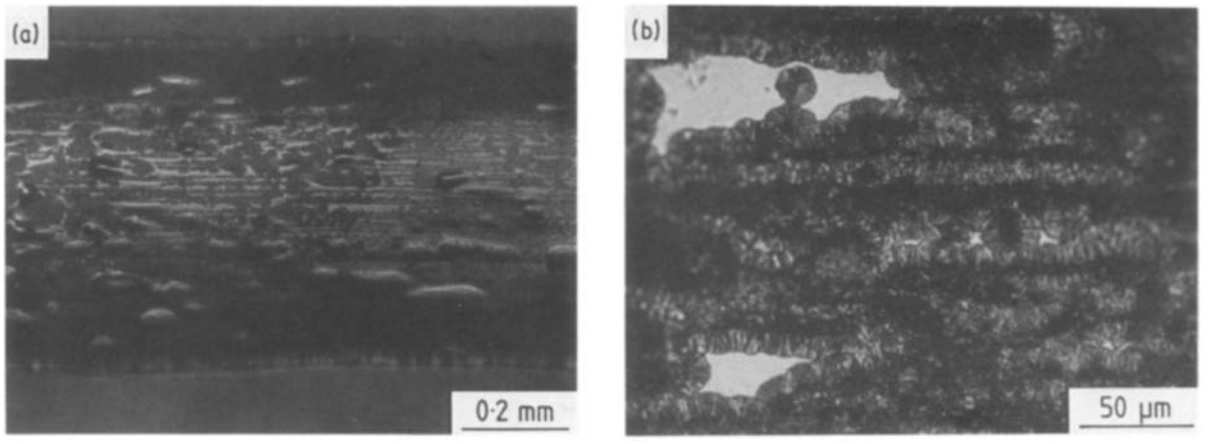

Figure 4 Optical micrographs of the etched wheel-side of ribbons annealed in argon: (a) 23 min at 623 K; (b) 3 h at 603 K. The bright areas in (b) are the untransformed surfaces of depressions.

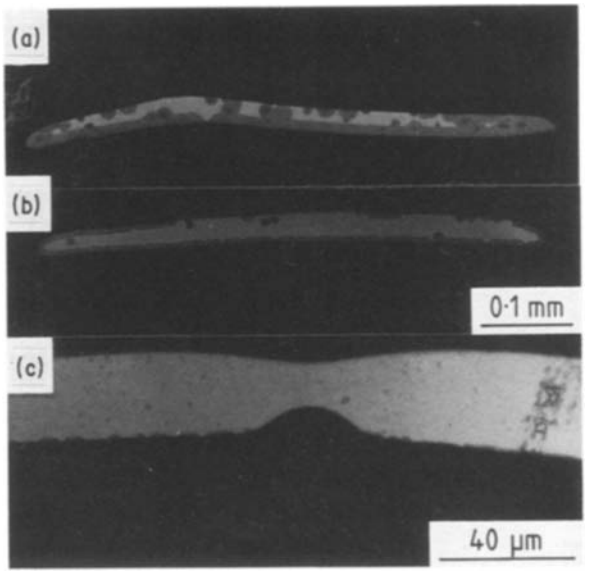

Figure 5 Etched cross-sections of ribbons annealed in argon: (a) 3 h at 603 K; (b) 30 min at 623 K; (c) 30 min at 603 K. In each case the wheel-side of the ribbon is at the bottom.

3.5. Effect of surface treatments

Given that surface heterogeneous nucleation is important and that there are significant differences in behaviour between the air- and wheel-sides, it is of interest to study the crystallization of ribbons with their original surface removed. This was done by etching in aqua regia. Fig. 8 shows the effect of subsequent annealing in argon. There is continuous planar growth from the surface, including the air-side and the depressions on the wheel side (compare Fig. 5a, with the same anneal). The etching has made uniform the properties of the surface and demonstrates that surface effects determine the pattern of crystallization. The copious nucleation induced by etching precludes the surface roughening seen in Fig. 3. Because the crystallization occurs equally on both sides, there is no tendency for the ribbon to curl (wheel-side concave) during annealing (Fig. 5b).

The enhancement of surface crystallization by etching could be attributed to selective oxidation, as suggested by Köster [4] in his work on $Fe_{40}Ni_{40}B_{20}$ described in Section 1. In contrast to Köster's finding, however, in the present case ion milling to remove the original surface ($\sim 3\,\mu m$ eroded) has exactly the same effect as etching. This suggests that oxidation may not be the cause of enhanced crystallization and anneals were carried out in different atmospheres to clarify this (next section). Whether caused by selective oxidation or otherwise, it is expected that a loss of phosphorus, leaving a metal-rich surface layer, might induce copious nucleation. A $0.5\,\mu m$ thick layer of polycrystalline $Pd_{50}Ni_{50}$ alloy was deposited by d.c. magnetron sputtering on to as-produced and ion-milled ribbons. It was found in each case that there was enhanced nucleation as seen, for example, in Fig. 8. Thus a metal enrichment at the surface does promote crystallization, presumably because the alloy deviates from the good glass-forming composition.

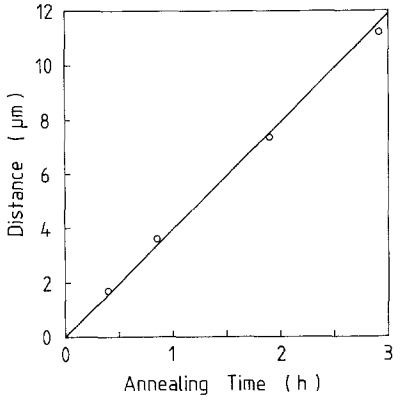

Figure 6 Extent of planar growth from the wheel-side of ribbon as a function of annealing time at 603 K (in argon). The constant growth rate is $1.1 \times 10^{-9}\,m\,sec^{-1}$.

3.6. Effect of annealing atmosphere

Ribbons annealed in vacuum showed continuous surface crystallization such as seen in Fig. 8. This was true of as-produced ribbons, and of ribbons pre-treated by etching or ion-milling. This suggests that loss of phosphorus by evaporation (faster in vacuum than in argon), rather than any oxidation, is responsible for enhancing surface crystallization.

The effect of oxidation was tested directly by annealing in air. Remarkably, the surface crystallization was greatly retarded, not only on as-produced ribbons, but also on those etched and ion-milled. Fig. 9 shows the wheel-side of untreated ribbon annealed in air for 3 h at 603 K. This should be compared with Fig. 4b (and Fig 5a), showing the effect of the same anneal in argon. That the preferential nucleation on the wheel-side can be so easily removed by annealing in air suggests that the nucleation was not due to contamination, but to a more subtle effect. The nucleation on annealing in air is not just retarded to the extent that the wheel-side behaviour resembles that expected for the air-side annealed in argon. The crystals shown on the wheel-side in Fig. 9 are not only few in number, but also much too small to have been growing since the beginning of the anneal. The delay or incubation time for the onset of crystal growth can be calculated and is about 2.25 h at 603 K.

More severe oxidation was caused by annealing in water vapour. This induced copious surface nucleation.

3.7. Discussion

Auger electron spectroscopy studies of the surfaces of as-produced ribbons do not show much difference between the sides, but there is somewhat more oxygen on the air-side. After annealing in argon the surfaces are found to be rich in nickel, with noticeable nickel depletion underneath. This suggests that a layer of NiO is formed at the surface. The results of annealing in air suggest that the formation of NiO must inhibit crystallization, and we propose that it does so by acting as a passive barrier layer preventing loss of phosphorus by evaporation or oxidation. (The loss of phosphorus does not have to be stopped, but merely made sufficiently slow that internal diffusion in the alloy can prevent serious phosphorus depletion just below the NiO layer.) This proposal is in broad agreement with all of our experimental findings.

Etching and ion-milling enhance crystallization by

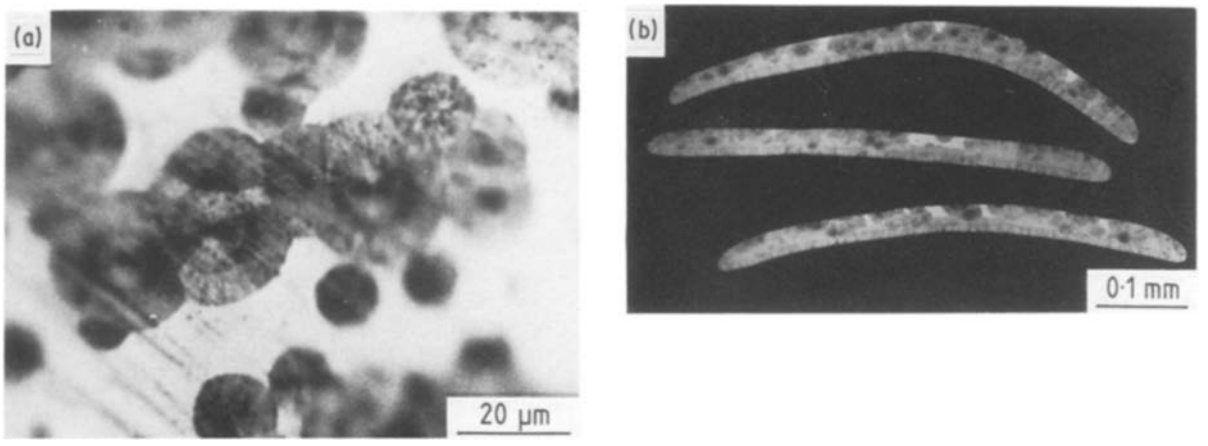

Figure 7 Optical micrographs of a ribbon annealed in argon for 30 min at 623 K, 15 h at 583 K, and 30 min at 623 K: (a) the air-side, etched; (b) etched cross-sections (with wheel-side at bottom).

removing any initial layer of protective NiO. Annealing in vacuum also enhances it by promoting evaporation of phosphorus and preventing further formation of oxide. Annealing in air clearly inhibits crystallization by promoting the formation of a protective layer, and it is possible that some oxidation also occurs on annealing in the not completely pure argon. Metal deposition enhances crystallization by preventing oxidation and providing a good sink for phosphorus.

On this model the behaviour of as-produced ribbons annealed in argon must imply more oxidation on the air-side. This is confirmed by the Auger results. There must also be more oxide on the depressions on the wheel-side, and less oxide near the ribbon edges on the air-side. How would such variations in the degree of oxidation of the surface arise? We suggest that they arise only from variations in quench rate. Regions of the ribbon which are quenched faster will have less time for oxidation during production. On the air-side the quench rate will be higher near the edges, both because the ribbon is thinner there and because of faster heat flow laterally into the quenching wheel. On the wheel-side the depressions will be more slowly cooled as they are not in contact with the wheel. The lower quench rate above these depressions cause the alloy to remain fluid for longer, resulting in depressions in the top surface. These also should be more slowly cooled and less likely to crystallize. There is perhaps some evidence for this in Fig. 1. Thus the differences in surface crystallization behaviour are attributed to differential oxidation and not to any prior contamination of the ribbons.

When there is severe oxidation, as in water vapour when a protective oxide is not formed, surface crystallization is enhanced, presumably because excess palladium builds up below the surface.

4. Conclusions

The easy glass-forming alloy $Pd_{40}Ni_{40}P_{20}$, made amorphous by melt-spinning in air, was chosen to study surface crystallization. While there is some internal nucleation and growth of crystals, the majority of the crystallization was at the surface. Surface crystallization is enhanced by removing the original surface (by etching or ion-milling), by annealing in vacuum, or by coating with metal. It is hindered by oxidation. This is in marked contrast to other metallic glasses for which selective oxidation, by changing the surface composition, promotes crystallization. In $Pd_{40}Ni_{40}P_{20}$ surface crystallization is most likely to be caused by loss of phosphorus, and this can be hindered by the formation of a protective NiO layer.

As-produced ribbon annealed in argon shows non-uniform surface crystallization: there is more crystallization on the wheel-side than on the air-side; on the air-side there is more near the edges; and on the wheel-side there is more in contact areas. This non-uniformity probably results from differential oxidation during production, and that, in turn, results from variations in quench rate. The specific sites at which the crystallization nucleates have not been identified, but clearly they are not randomly distributed. An analysis of the crystal size distribution shows that

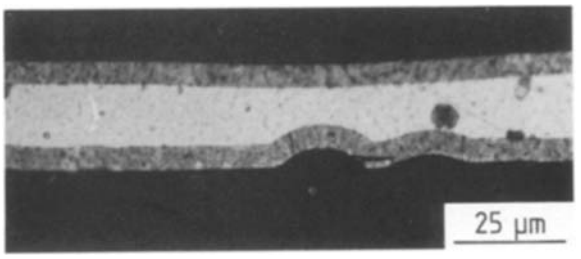

Figure 8 Etched cross-section of ribbon annealed for 3 h at 603 K in vacuum. To be compared with Fig. 5a (annealed in argon).

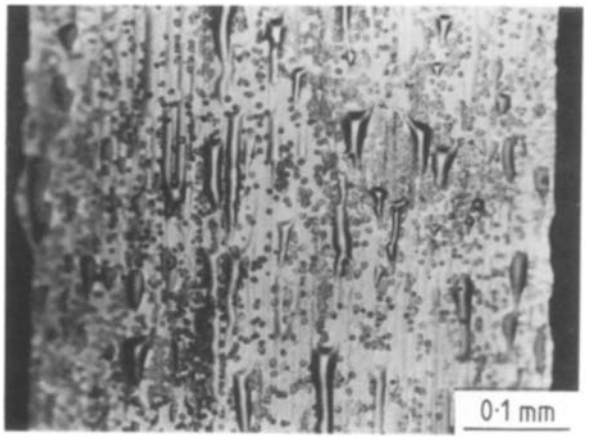

Figure 9 Etched wheel-side of ribbon annealed in air for 3 h at 603 K. To be compared with Fig. 4b (3 h at 603 K in argon).

there is saturation of heterogeneous sites. The distribution of these sites, often in lines parallel to the ribbon length, may indicate some contamination arising in production.

When surface nucleation is sparse, relief develops as the remaining liquid is drawn in between the growing crystals. On the other hand, when the nucleation is copious, the resulting planar growth enables straightforward measurement of the crystal growth rate, which as expected depends only on the temperature. Because well-defined crystalline layers with highly directional growth can be produced, a potential for microstructural control by devitrification has been demonstrated. Complex annealing treatments show the possibility of marking stages in the crystallization process.

Acknowledgements

A.G.E. is grateful to the British Council for financial support. We thank J. L. Sacedón (C.S.I.C., Madrid) for help with Auger analysis, J. E. Rout, P. V. Evans, P. E. Donovan and R. E. Somekh for experimental assistance, and Professor D. Hull for the provision of laboratory facilities.

References

1. H. N. OK and A. H. MORRISH, *Phys. Rev. B* **23** (1981) 1835.
2. J. L. WALTER, *J. Appl. Phys.* **36** (1965) 1213.
3. G. GROSS, R. B. STEPHENS and D. TURNBULL, *ibid.* **48** (1977) 1139.
4. U. KÖSTER, in "Amorphous Metals and Non-Equilibrium Processing", edited by M. von Allmen (Les Editions de Physique, Paris, 1984) p. 175.
5. A. J. DREHMAN, A. L. GREER and D. TURNBULL, *Appl. Phys. Lett.* **41** (1982) 716.
6. H. W. KUI, A. L. GREER and D. TURNBULL, *ibid.* **45** (1984) 615.
7. P. E. DONOVAN, P. V. EVANS and A. L. GREER, *J. Mater. Sci. Lett.* **5** (1986) 951.
8. P. V. EVANS, A. GARCIA ESCORIAL, P. E. DONOVAN and A. L. GREER, *Mater. Res. Soc. Symp. Proc.* **57** (1986) in press.
9. A. J. DREHMAN and A. L. GREER, *Acta Metall.* **32** (1984) 323.

Received 4 February
and accepted 15 April 1987